

NUMERICAL SIMULATION OF ANISOTROPIC ABLATION OF SILICEOUS CONCRETE – ANALYSIS OF CCI-3 MCCI EXPERIMENT BY MPS METHOD

Xin Li and Akifumi Yamaji

Waseda University

3-4-1 Okubo, Shinjuku-ku, Tokyo 169-8555, Japan

lixin@fuji.waseda.jp; akifumi.yamaji@waseda.jp

ABSTRACT

The molten corium-concrete interaction (MCCI) phenomenon was analyzed with the Moving Particle Semi-implicit (MPS) method by carrying out a numerical simulation of CCI-3 experiment. The interaction of the fully oxidized PWR core melts with a specially-designed two-dimensional siliceous concrete test section was analyzed, focusing on investigating the anisotropy in cavity ablation with siliceous concrete. The phase transition of the melt and the concrete was modeled based on a phase transition model for mixture. The effects of aggregates on the lateral and axial ablation were investigated by simulating two specially designed cases: one with aggregates in concrete and the other without aggregates in concrete. The simulation results by MPS method reproduced the anisotropic cavity ablation profile and the overall axial and lateral ablation rates agreed well with the experimental measures. The experimental and MPS results both indicated that the crust on the interface between the basemat and melt pool played an important part in axial concrete ablation process by hindering the axial ablation. The simulation results by MPS method also provided an evidence to support the theory that aggregates were the cause of anisotropic ablation profile in cavity with siliceous concrete because aggregates could delay the axial basemat ablation more significantly than the lateral one and influence the power split in the melt pool.

KEYWORDS

MCCI; MPS method; Siliceous concrete ablation; Aggregates

1. INTRODUCTION

In a severe accident, the late containment failure may be caused by the thermal attack of core melt on the reactor pit or concrete basemat. The core melt or molten corium which is discharged from the failed reactor vessel could drop on and interact with the concrete basemat. This so-called Molten Corium Concrete Interaction (MCCI) phenomenon could lead to gradual ablation of the basemat and sidewalls of the reactor pit and jeopardize the integrity of containment if it is not terminated, namely when corium is cooled down to the temperature below that for concrete ablation. The consequences can be rather catastrophic since there is potential risk that a large amount of fission products will release to the environment. In the light of this consequence, the trigger and development of MCCI should be investigated intensively to mitigate and prevent its consequences.

In MCCI, the main issue that needs to be addressed is when and how the molten corium will melt through the basemat. Thus concrete behavior under high temperature and its ablation should be investigated and

studied. A number of MCCI experiments have been carried out since 1980s. The early large scale experiments, such as SURC [1][2], SWISS [3], ACE [4], and MACE [5], are all one-dimensional MCCI experiments, mainly aiming at analyzing one-dimensional ablation behavior of oxidic corium or metal with concrete, the effect of Zr oxidation on MCCI, and the effect of an overlying water pool. More recent MCCI experiments began to focus on the two-dimensional concrete ablation pattern with respect to the axial versus radial ablation ratio and melt coolability induced by late water injection. In a series of CCI experiments performed by OECD/NEA [6], one of the major findings was that the ablation in siliceous concrete tended to present an anisotropic pattern, in which the radial ablation was more significant than the axial ablation. On the other hand, the tests with limestone concrete showed a more isotropic ablation pattern, in which the radial and axial ablations tended to be similar. Since the ablation depth in the concrete cavity is an important parameter regarding concrete integrity, it is necessary to understand the mechanism of the ablation patterns in different types of concrete in order to maintain the containment integrity in case of MCCI. As to the isotropic and anisotropic ablation patterns regarding limestone-rich and silica-rich concretes, one explanation is that these two types of concrete use different aggregates as constituent materials. Generally, concrete is a mixture of mortar (a mixture of cement, water and fine aggregates) and gravel (large aggregates), or a mixture of cement paste and aggregates (sand and gravel). Limestone concrete is composed of limestone aggregates (CaCO_3) which would decompose into CaO and CO_2 at a temperature of 973-1173K. On the other hand, the siliceous concrete is composed of silica aggregates, which is thermally stable at 2000K. Due to the apparently different behavior of aggregates at high temperature, one explanation to the anisotropic ablation in siliceous concrete is that this phenomenon may be caused by the existence of relatively stable aggregates (silica) that still remain solid and stable at concrete melt temperature on the axial cavity bottom, which act as cold sources in the corium pool thus contributing local crust on the basemat surface preventing downward/axial ablation and leading to a tendency of much easier and pronounced lateral sidewall ablation. However, additional experiments and analysis are needed to support this theory.

Meanwhile, several computer codes have also been developed and validated against the experimental results, such as CORCON [7], WECHSL [8], CORQUENCH [9], COSACO [10], ASTEC/MEDICIS [11] and TOLBIAC-ICB [12]. These codes were developed in the aim of modeling the physical and chemical phenomena during MCCI. In these codes, the corium pool is described with different heat transfer correlations, the pool stratification models, the cavity ablation models and the pool/concrete interface models. Previous code validations against experiments and benchmark calculations have shown discrepancies on the axial and lateral ablation among these codes, and still uncertainties remain in the prediction of the shape of the ablated cavity [13][14]. The large discrepancies indicate the limitations of specific correlations and models that are used in the codes, which suggest a necessity to develop a multi-dimensional code based on fundamental governing equations to further improve the accuracy and reliability of numerical analysis.

The MPS method, which is known as the Moving Particle Semi-implicit method, was first proposed by Koshizuka and Oka in 1990s. In the MPS method, the basic governing equations are discretized based on particle interactions. Large deformation of interfaces and phase change processes can be easily simulated since no grids are needed [15]. Through the past years, the MPS method has been applied in a wide range of engineering applications including nuclear engineering [16][17][18], chemical engineering [19] and ocean engineering [20]. Especially in nuclear engineering, the MPS method has been validated and proved effective to analyze a number of phenomena in a severe accident scenario, especially the analysis that involves phase change in melt behavior, such as molten core spreading [21], stratification and solidification/melting behaviors [22], melt penetration and freezing behavior in an instrument tube [23][24]. Moreover, MPS method has also been successfully applied to analyze one-dimensional MCCI experiments SURC-2 and SURC-4 [25]. Simulation by MPS method employs basic physical models such as heat conduction, melting, solidification, viscosity, surface tension, which provides a more fundamental

approach to understand physical process. In the light of these successful implementations, applicability of MPS method for the severe accident analysis is very feasible and effective.

In this paper, numerical simulation of two-dimensional MCCI experiment CCI-3 was performed by a two-dimensional computer code developed in the frame of MPS method, providing a direct numerical modeling of the interaction of the fully oxidized PWR core melts with a two-dimensional siliceous concrete test section during CCI-3. The characteristic moments of the dry cavity ablation process and the axial/radial ablation front/rate were presented. The effect of the aggregates which were believed to be the cause of anisotropic ablation pattern in siliceous concrete was also discussed in detail.

2. NUMERICAL METHOD

2.1. MPS Method

The mass, momentum and energy conservation equations applied in MPS method are:

$$\frac{D\rho}{Dt} = 0 \quad (1)$$

$$\rho \frac{D\mathbf{u}}{Dt} = -\nabla P + \mu \nabla^2 \mathbf{u} + \rho \mathbf{g} \quad (2)$$

$$\frac{\partial H}{\partial t} = k \nabla^2 T + Q \quad (3)$$

In MPS method, all the differential operators are substituted according to the following particle interaction models. The common kernel function used to discretize the differential operators is defined as:

$$w(r) = \begin{cases} \frac{r_e}{r} - 1 & 0 \leq r < r_e \\ 0 & r_e \leq r \end{cases} \quad (4)$$

where r is the distance between particles, and r_e is the effective interaction radius for narrowing down the scope of interaction. The particle number density n_i at the position \mathbf{r}_i , which is defined as the summation of the weight function value and is proportional to the fluid density, is defined as:

$$n_i = \sum_{j \neq i} w(|\mathbf{r}_j - \mathbf{r}_i|) \quad (5)$$

The gradient model and Laplacian model that are used to discretize the gradient and Laplacian operators are shown in Eqs. (6) and (7).

Gradient model:

$$\langle \nabla \varphi \rangle_i = \frac{d}{n_i} \sum_{j \neq i} \left[\frac{\varphi_j - \varphi_i}{|\mathbf{r}_j - \mathbf{r}_i|^2} (\mathbf{r}_j - \mathbf{r}_i) w(|\mathbf{r}_j - \mathbf{r}_i|, r_{e,ij}) \right] \quad (6)$$

Laplacian model:

$$\langle \nabla^2 \varphi \rangle_i = \frac{2d}{\lambda_i n_i} \sum_{j \neq i} [(\varphi_j - \varphi_i) w(|\mathbf{r}_j - \mathbf{r}_i|, r_{e,ij})] \quad (7)$$

where $\lambda_i = \frac{\sum_{j \neq i} w(|\mathbf{r}_j - \mathbf{r}_i|) |\mathbf{r}_j - \mathbf{r}_i|^2}{\sum_{j \neq i} w(|\mathbf{r}_j - \mathbf{r}_i|)} \cong \frac{\int_v w(r) r^2 dv}{\int_v w(r) dv}$

2.2. Phase Transition Model

Since melting and solidification processes of materials are the main concerns during MCCI, phase transition is modeled with respect to the state of change of each particle in MPS method. Each particle is characterized by temperature T , enthalpy h and solid fraction γ . The temperature of the particle is calculated as a function of enthalpy, which is:

$$T = \begin{cases} T_s + \frac{h - h_{s0}}{\rho C_{ps}} & h < h_{s0} \\ T_s + \frac{T_l - T_s}{h_{s1} - h_{s0}} (h - h_{s0}) & h_{s0} \leq h \leq h_{s1} \\ T_l + \frac{h - h_{s1}}{\rho C_{pl}} & h_{s1} < h \end{cases} \quad (8)$$

The solid fraction of the particle is defined as:

$$\gamma = \begin{cases} 1 & h < h_{s0} \\ \frac{h_{s1} - h}{h_{s1} - h_{s0}} & h_{s0} \leq h \leq h_{s1} \\ 0 & h_{s1} < h \end{cases} \quad (9)$$

When $\gamma = 0$, the particle is in a completely fluid state; when $\gamma = 1$, the particle is in a completely solid state; when $0 < \gamma < 1$, the particle is in a partially fluid and partially solid state. Analysis of melt spreading experiments for stainless steel SPREAD suggested that about 55% of heat of fusion needs to be removed from the melt (i.e. containing 55% solid fraction) to stop the spreading process [26]. This indicated that a critical value of solid fraction to determine when molten materials change from the fluid to solid is important.

2.3. Viscosity Model for Corium Mixture

The viscosity of molten corium and concrete mixture is an important parameter to predict its rheological behavior during MCCI. Since the viscosity of molten corium and concrete mixture has strong dependence on temperature, especially between the solidus and liquidus temperature of corium, a temperature dependent model was used in current MPS code. The viscosity measurement was conducted with 27.5 weight-% siliceous concrete and analyzed by Epstein [27], and could be correlated as follows:

$$\mu = \begin{cases} 5.187 \cdot 10^{-17} \cdot e^{82230/T}, & 2000\text{K} < T < 2284\text{K} \\ 1.275 \cdot 10^{-5} \cdot e^{22200/T}, & 2284\text{K} \leq T < 2600\text{K} \end{cases} \quad (10)$$

The viscosities for over 2600K and less than 2000K were deemed as constant values calculated from the above correlations at 2000K and 2600K, respectively.

2.4. Numerical Calculation Procedure

In MPS method, a semi-implicit algorithm is employed. The viscosity term and gravity term from Equ.2 and the temperature are explicitly calculated, while the pressure gradient term is implicitly calculated. In each time step, the momentum equation is first explicitly solved to obtain the temporal velocities and positions except the pressure gradient term. Then the pressure is calculated implicitly with the following Poisson equation of pressure (Eq. 11) deduced from the mass conservation equation to maintain the incompressibility of the fluid. Then the positions and velocities of the particles are corrected by the pressure gradient as shown in Eqs. 11-13. A calculation flowchart for the MPS algorithm is shown in Fig.1.

$$\langle \nabla^2 P \rangle^{k+1} = -\frac{\rho^0}{\Delta t^2} \frac{n^* - n^0}{n^0} \quad (11)$$

$$\mathbf{u}^{k+1} = \mathbf{u}^* - \frac{\Delta t}{\rho^0} \nabla P \quad (12)$$

$$\mathbf{r}^{k+1} = \mathbf{r}^* - \frac{\Delta t^2}{\rho^0} \nabla P \quad (13)$$

3. TEST AND SIMULATION CONDITIONS

3.1. CCI-3 Experiment Description

Core-Concrete Interaction (CCI) experiments consisted of a series of large scale reactor materials experiments performed within the OECD/MCCI program in order to address remaining uncertainties related to long-term two-dimensional corium-concrete interaction under both wet and dry cavity conditions [6]. CCI-3 experiment was designed to investigate the interaction of a fully oxidized Pressurized Water Reactor (PWR) core melt, initially containing 15 weight-% siliceous concrete, with a specially designed two-dimensional siliceous concrete test section. The siliceous concrete for this test was European type. The compositions of core melt and concrete are shown in Tables 1 and 2, respectively. The apparatus for containment of the core material consists of a test section that is about 3.4 m tall with a square internal cross-section which initially measures 50 cm x 50 cm. The principal components of the test section consist of a bottom support plate, two sidewall sections, one basemat section and an upper enclosure lid. A side view and top view of the lower part of the test section are shown in Figs. 2 and 3, respectively. The concrete basemat is initially 55 cm deep and each of the two concrete sidewalls is 56.2 cm thick, which provides 20 cm of remaining sidewall thickness once the 35 cm axial and lateral ablation limits have been reached. A video camera was installed on the upper lid of the test section to record the visual information regarding the corium-concrete interaction and melt quenching behavior. Type K and Type C thermocouple assemblies were instrumented into the concrete sidewalls and basemat to record the temperature data regarding the two-dimensional ablation profile and melt as a function of time. The main test conditions and procedures are listed in Table 3.

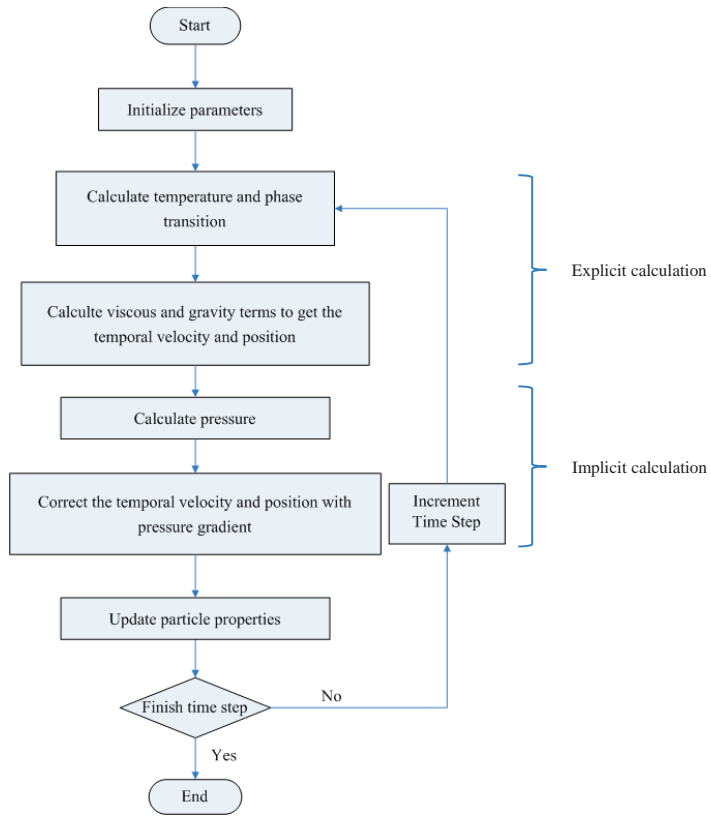


Figure 1. MPS algorithm flowchart

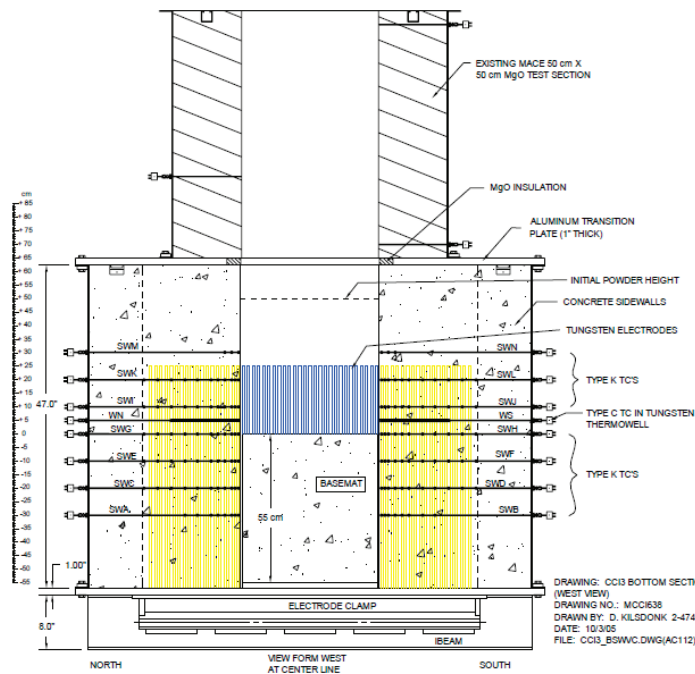


Figure 2. The lower part of CCI-3 test section: side view [6]

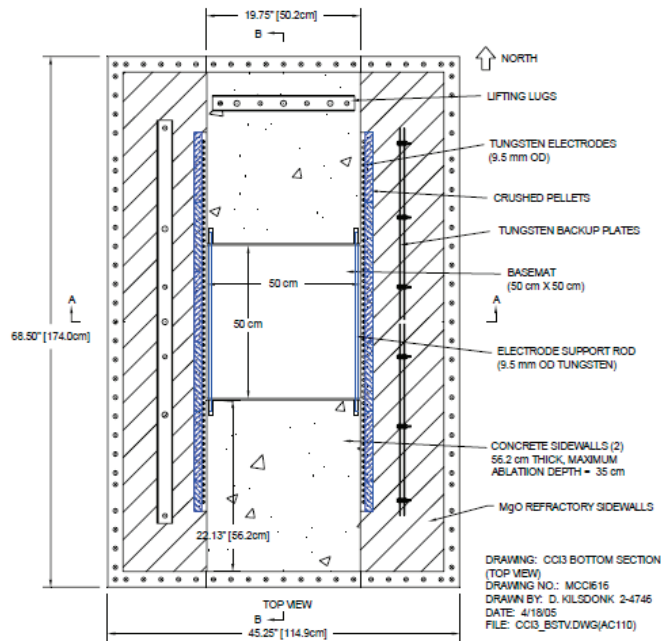


Figure 3. Top view of the test section of CCI-3 [6]

Table I. Melt composition in CCI-3 [6]

Composition	UO ₂	ZrO ₂	Calcined Concrete*	Cr
Weight percent (%)	56.32	23.13	14.14	6.41

*Calcined concrete: 79.0/0.9/15.6/4.5 weight-% SiO₂/MgO/CaO/Al₂O₃

Table II. Main chemical composition of the siliceous concrete used in CCI-3 [6]

Composition	SiO ₂	CaO	Al ₂ O ₃	Fe ₂ O ₃	MgO	K ₂ O	Na ₂ O	SO ₃	TiO ₂
Weight percent (%)	59.91	16.79	3.53	1.49	0.85	0.81	0.66	0.434	0.155

Table III. Test procedures of CCI-3 [6]

Time(minute)	Major events of CCI-3
-0.7	Thermite burn initiated.
0.0	Melt generation completed; initial temperature ~1950 °C
0.0-0.8	Onset of basemat ablation detected in the SE basemat quadrant, and at 0.0, +10.0, +20.0, and +30.0 cm elevations on both concrete sidewalls.
1.6	Target input power of 120 kW reached.
51.4	Onset of sustained basemat ablation detected at all instrument locations.
107.6	Sidewall ablation reaches 29.2 cm in South wall at +10.0 cm elevation; water injection initiated; end of dry cavity ablation
140.3	Lance used to breach the crust. No noticeable increase in the debris cooling rate.
143.1	Ablation reaches 34.3cm limit at the +10 cm elevation in the South sidewall.
146.4	Power supply operation terminated.
173.3	Data logging terminated.

3.2. Simulation Conditions of CCI-3 experiment

In order to model CCI-3 experiment, two cases were carried out with two slightly different initial particle configurations as shown in Fig. 4. These two particle configurations with the same geometry were almost the same with the only difference lying in whether there existed aggregates in the concrete. The purpose of building these two different particle configurations and carrying out two simulation cases was to identify the effect of aggregates on MCCI since aggregates were believed to account for the anisotropic ablation profile in cavity for MCCI experiments with siliceous concrete. Since the geometry of the test section in CCI-3 is symmetrical, only half of the real test section geometry was built in consideration of computational cost. Five types of particles were used to represent different materials in the geometry, namely the melt, the concrete, the aggregate and two types of wall particles. The aggregate particles were considered to distribute evenly within the concrete. Additionally, another two types of particles were set to represent the solidified melt (crust) and the molten concrete for phase transition simulation. The bulk of MgO sidewalls were described with dummy wall particles, and wall particles were applied on the layer that immediately contacted with the melt and concrete. The difference between these two types of wall particles is that the pressure was set to be 0 and not calculated for dummy wall particles, while the pressure of wall particles was calculated in each time step. Meanwhile, nonslip boundary condition was applied on this layer of wall particles. The left sidewall was deemed as adiabatic during simulation. A detailed description of the initial physical properties of the materials is listed in Table 4. The physical properties of the melt, concrete and silica aggregates referenced several literatures on physical properties for these materials [28] [29], and temperature dependence was taken into consideration during simulation. Here the same physical properties for concrete were applied in both cases considering concrete as a mixture in general. In this way, the influence of the aggregates could be better presented although in the real situation the concrete should be considered as a mixture of mortar and aggregates. The initial conditions of simulation for CCI-3 were listed in Table 5. Since the MPS simulation only considered dry cavity ablation, the simulation time is 107.6 minutes (6426.0 seconds).

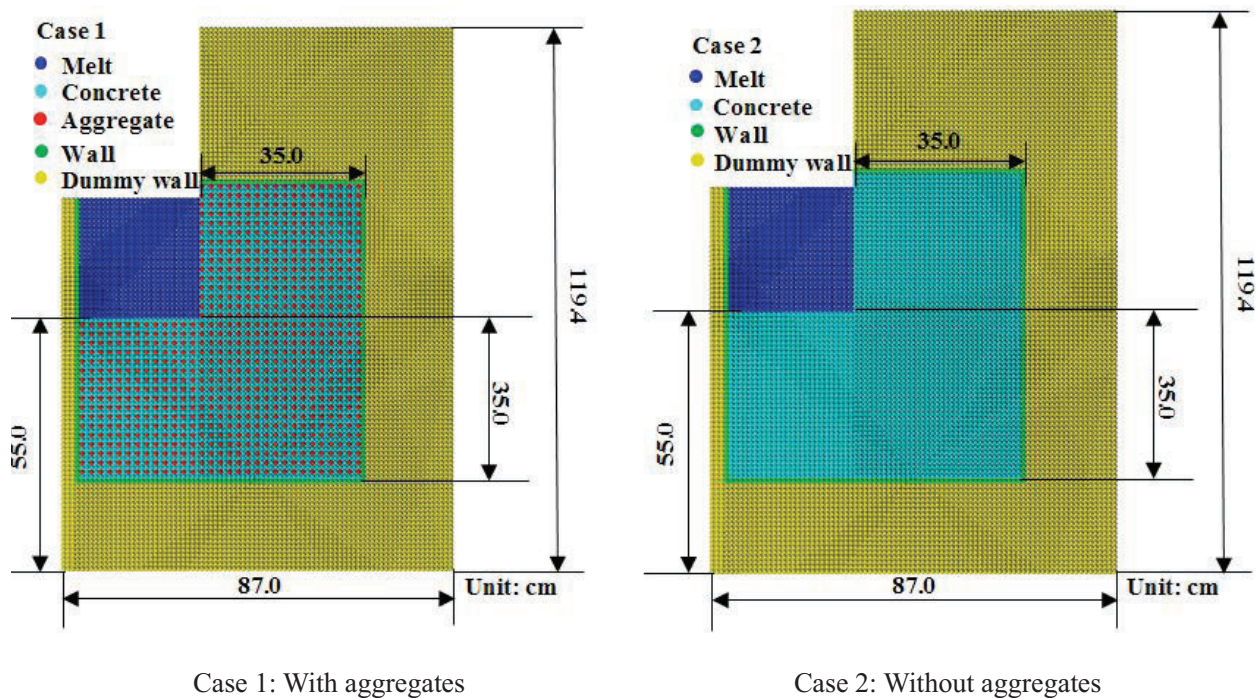


Fig.4 Initial particle configuration for CCI-3 simulation

Table IV. Initial physical property of the materials

Property	Corium (PWR core melt, with 15 wt-% siliceous concrete)	Concrete (siliceous, 300K)	Aggregate (silica, 300K)	MgO (300K)
Density (kg/m ³)	6500.0	2270.0	2650.0	2680
Specific heat (J/kg·°C)	550.0	845.2	782.6	1250
Heat conduction coefficient (W/m·K)	4.0	2.5 (<1073K) 1.3 (≥1073K)	3.0	6.7
Solidus temperature (K)	1573.0	1373.0		
Liquidus temperature (K)	2573.0	1523.0		
Latent fusion heat or decomposition heat (kJ/kg)	300.0	1800.0		

Table V. Initial conditions for CCI-3 simulation

Parameters	CCI-3
Particle size (Initial average distance between particles) (m)	0.008
Simulation time (s)	6460.0
Total particle number	8920
Initial melt temperature (K)	2223.0
Initial concrete temperature (K)	300.0
Input power (kW)	120.0

4. RESULTS AND DISCUSSIONS

Figure 4 shows a series of representative figures depicting the simulated progression of MCCI in the CCI-3 experiment. Two sets of figures are shown for Case 1 (with aggregates) and Case 2 (without aggregates). From the figures, it can be seen that both cases presented an anisotropic profile in the cavity at the end of simulation, in which the lateral sidewall ablation was much more significant than the axial basemat ablation. This agreed with the post-test view of final cavity shape in CCI-3 experiment. The sidewall ablation occurred at 250s and 260s for Case 1 and Case 2, respectively while the basemat ablation did not occur until at 3500s and 3210s for Case 1 and Case 2, respectively. The delay of the basemat ablation was caused by the thick crust that is formed on the interface between the melt pool and the basemat at the very first beginning of the simulation. In the simulation, it was assumed that crust formed only on the interface between the melt pool and the basemat, namely no crust would develop along the sidewall. This assumption was made based on the observation that CCI-3 experiment showed evidence of initial crust formation on the concrete basemat, but there was no evidence of initial sidewall crust formation for this test. For both cases, the crust did not break until the late phase of the experiment. This so-called incubation period during which the ablation rate is very low plays an important part in MCCI. It is noted that the crust broke only due to heat transfer while there should be some slight chemical dissolution caused by molten concrete. This was neglected in current simulation since the crust dissolution was much less rapid for siliceous concrete than limestone concrete [30]. The duration of the incubation period was longer in Case 1 than that in Case 2. This is probably one of the effects that aggregates have on MCCI because aggregates are more thermally stable than concrete. Although the concrete that was in intermediate contact with the crust could still be ablated by the crust of high temperature, there was an obvious delay on the concrete ablation progression because the heat conduction between crust and concrete was much smaller than that between the fluid corium melt and concrete. The fluid corium melt could create a convective effect on the concrete that contacted with it, which could

enhance the heat transfer between the melt and concrete, and lead to faster ablation than for the crust and concrete.

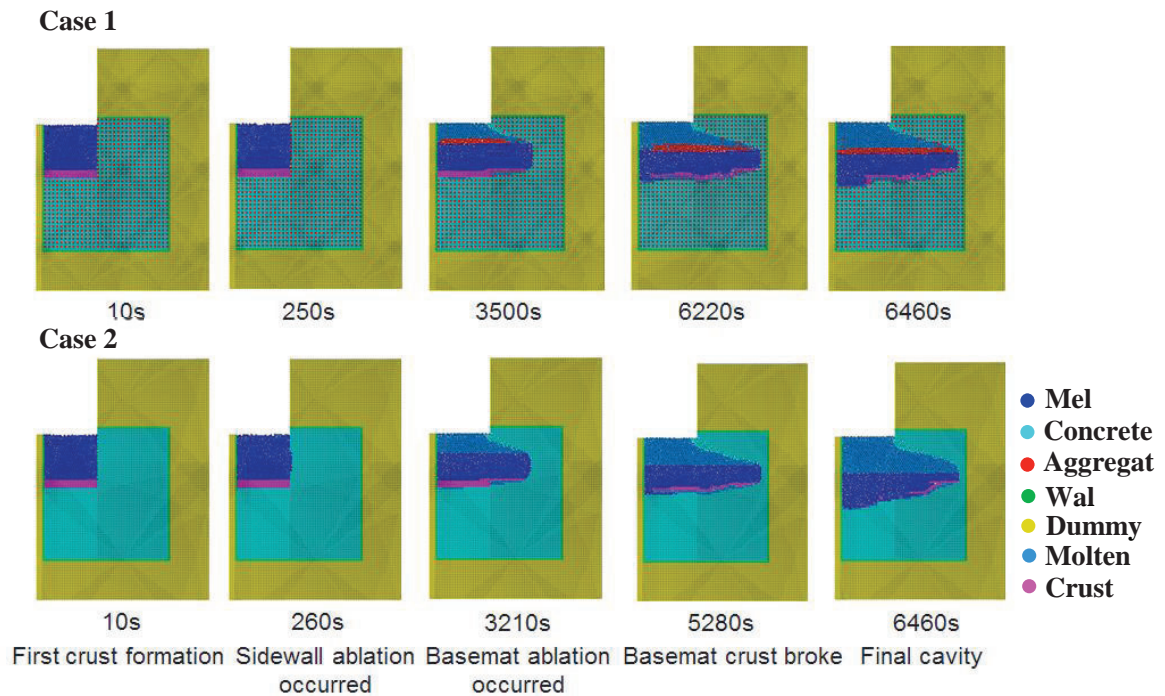


Figure 5. Representative moments of simulated MCCI process in CCI-3 experiment

For the final melt pool, stratification behavior was observed in both cases. Two zones can be clearly recognized: a corium melt phase immediately over the basemat and an overlying molten concrete phase. For Case 1, there was another phase comprised of aggregates between the corium melt phase and the molten concrete phase. This phenomenon agrees with the post-test observation of CCI-3 experiment. The post-test observation indicated that two zones appeared to be present: a heavy monolithic oxide phase immediately over the basemat that was enriched in core oxides, with a second overlying porous, light oxide phase that was enriched in concrete oxides for siliceous concrete tests. This stratification behavior was caused by the density difference between the materials. After melting, the molten concrete and aggregate particles with lower density compared to corium melt gradually rose, merged into the melt pool, floated and occupied the upper part of the melt pool.

The simulated axial and lateral ablation fronts of Case 1 and Case 2 are compared with experimental measurements in CCI-3 as presented in Fig.5. The lateral ablation fronts progressed much more quickly than the axial ablation fronts. For lateral ablation, Case 1 and Case 2 presented rather similar trend with Case 2 having a slightly faster ablation rate. The ablation rate was quite steady before basemat crust broke while decreased significantly after basemat crust broke. The basemat crust break gave rise to a sudden increase in axial ablation rate, which resulted in the decrease in the lateral ablation during the last 1000 seconds of the simulation. The final lateral ablation fronts (depths) of Case 1 and Case 2 were almost the same, which were 32cm each and slightly higher than the experimental measurement 29.2cm at the end of the dry cavity ablation. On the other hand, the axial ablation rate remained relative low compared to the lateral one. The axial ablation rates of Case 1 and Case 2 remained steadily low and came to a significant rise after 6220s and 5280s, respectively. This was exactly when basemat crust broke for both cases. In both cases, the basemat crust never formed again after the break. The final axial ablation front (depth) of Case 2 reached 10cm and was twice as much as that of Case 1. This indicated that the aggregates did have

an effect of slowing down the axial ablation, which provides evidence to support the theory that the aggregates have an effect on the anisotropic ablation profile with siliceous concrete considering that they could slow down the axial ablation. The reason why there is such delay in basemat crust break and slight delay in sidewall ablation could be perceived as that the aggregates have a higher thermal conductivity than concrete, which could influence the power split in the melt pool. As aggregates of higher thermal conductivity could gain more heat from the corium material than concrete, the heat that was distributed to the crust and concrete was less in Case 1 than Case 2, which resulted in later crust break and slower lateral ablation in Case 1.

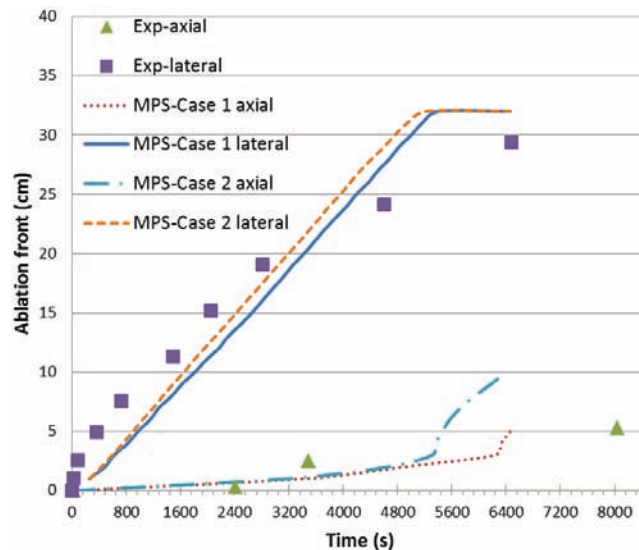


Figure 6. Axial and lateral ablation fronts of MPS simulation and CCI-3 experimental measures

The MPS predicted and experimental average ablation rate of CCI-3 are shown in Table 6. For lateral ablation, the dry cavity ablation process can be divided into two phases, which is marked by the time around 2800s when axial basemat ablation began. The lateral ablation rate after axial basemat ablation began (after 2800s) was slowed down by the commencement of increase in axial basemat ablation rate. The lateral ablation rate before 2800s predicted by MPS method for Case 1 and Case 2 are lower than that of the experimental measurement, while the lateral ablation rate after 2800s predicted by MPS method for both cases are higher than that of the experimental measurement. In general, considering the whole dry cavity ablation process, namely during first 6460s of CCI-3 experiment, the overall average ablation rate predicted by MPS method agrees well with the value calculated from experimental measurements. For axial ablation rate, the overall average lateral ablation rate is about 6 times of the overall average axial ablation rate. The axial ablation rate of Case 1 was close to the experimental measurement while that of Case 2 was twice as much as the experimental measurement. This indicated that aggregates could hinder the axial basemat ablation, which is believed to be the main cause of the anisotropic ablation profile with siliceous concrete. Meanwhile, due to the slight difference of lateral ablation rate before and after 2800s, the aggregates also have an influence on lateral ablation rate. However, the effect is not as obvious as that on the axial ablation rate. As previously discussed, this is caused by the difference in thermal conductivities of aggregates and concrete. The difference of influence on axial and radial ablation rate is due to the different amount of aggregates that was embedded in each layer of the concrete block and that was gradually accumulated in the melt pool. With more aggregates being gradually released into the melt pool as ablation progressed, the difference of radial ablation rates of Case 1 and 2 gradually increased, which indicated more heat was dissipated to aggregates floating in the melt pool rather than sidewall and basemat crust in Case 1 than in Case 2. This again demonstrated the influence of aggregates on power split in MCCI.

Table VI. Experimental and MPS predicted concrete ablation rate for CCI-3

Average ablation rate (cm/h)	Experiment	MPS (Case1-With aggregates)	MPS (Case2-Without aggregates)
Lateral (before 2800s)	24.4	20.6	22.5
Lateral (after 2800s)	10.2	15.7	14.0
Lateral (in overall)	16.3	17.8	17.8
Axial	2.5	2.8	5.6

5. CONCLUSION

In this paper, a two-dimensional code for MCCI analysis was developed in the frame of MPS method. Based on basic governing equations and less use of empirical correlations compared to other conventional MCCI codes, the developed code was successfully applied to the numerical simulation of CCI-3 experiments intended to investigate the interaction of fully oxidized PWR core melts with two-dimensional siliceous concrete test section. The following conclusions can be drawn from the present study:

1. The MPS simulation results presented an anisotropic profile in cavity at the end of simulation, which reproduced and agreed well with the post-test observation of cavity shape in CCI-3 test. The overall lateral and axial ablation rates evaluated from the MPS simulation results matched well with the experimental measurements, but the detailed ablation front history by MPS simulation had some deviation from the experimental measurements. The MPS simulation results showed that the overall average lateral ablation rate was about 6 times that of the average lateral ablation rate, which was also consistent with the experimental observation.
2. Crust on the interface between the basemat and melt pool plays an important part in axial concrete ablation process. According to MPS simulation, the major delay of axial ablation was caused by the crust formation on the interface between the basemat and melt pool. Once the crust broke, the axial ablation rate began to increase dramatically and the lateral ablation rate correspondingly decreased because of the change in lateral and axial power split. More study is needed to extrapolate current conclusion to plant scale. In real plant-scale MCCI, crust formation and break is also crucial to determine the progression of MCCI. However, the crust stability and break mechanism for real plant cavity needs more research and study.
3. Aggregates have an influence on both the axial and lateral ablation rate according to the analysis of the different MPS results for CCI-3 experiments: the cases with and without aggregates. The differences in average axial ablation rate between these two cases indicated that aggregates could hinder the axial ablation, while the influence on lateral ablation rate was not as obvious as on the axial one. The influence of the aggregates on power split in MCCI was also presented. Due to the higher thermal conductivity and density, aggregates could count for more power consumption than concrete.

NOMENCLATURE

C_p	specific heat, J/(kg·K)	J/ kg
d	dimension number	H thermal energy, J/ m ³
g	gravity acceleration, m/s ²	m mass, kg
h	enthalpy, J/ kg	n particle number density
h_{s0}	enthalpy when melting begins, J/ kg	P pressure, Pa
h_{s1}	enthalpy when melting completely ends,	Q heat source, W/m ³
		r particle location vector

r	particle distance, m	u	particle velocity vector
T	temperature, K	w	weight function
t	time, s		

Greek letters

φ	Scalar variable	ρ	density, kg/m ³
λ	coefficient	μ	viscosity, Pa·s

Superscript/subscript

e	effective	n, n-1	designation of time step
i,j	particle number	0	initial condition
l	liquidus	s	solidus
*	temporal		

ACKNOWLEDGMENTS

The professional guidance and help from Dr. Yoshiaki Oka, Emeritus Professor of the University of Tokyo, is highly appreciated. The MPS code of the present study was developed based on the original code, MPS-SW-Main-Ver2.0 that was kindly provided by S. Koshizuka and K. Shibata (Koshizuka, S and Shibata, K, 2006). The financial support from China Scholarship Council through offering scholarship to the first author is gratefully acknowledged.

REFERENCES

1. E.R. Copus et al., "Core-Concrete Interactions Using Molten Steel with Zirconium on a Basaltic Basemat: The SURC-4 Experiment," NUREG/CR-4994, Sandia National Laboratories, Albuquerque, NM (1989).
2. E.R. Copus, R.E. Blose, J.E. Brockmann et al., "Core-Concrete Interactions Using Molten UO₂ with Zirconium on a Basaltic Basemat, The SURC-2 Experiment," Sandia National Laboratories, Report NUREG/CR-5564, SAND90-1022 (1992).
3. R.E. Blose, J. E. Gronager, A. J. Suo-Anttila et al., "SWISS: Sustained Heated Metallic Melt/Concrete Interaction with Overlying Water Pools," NUREG/CR-4727, SAND85-1546 (1987).
4. D.H. Thompson et al., "Thermal Hydraulic Aspects of the Large-scale Integral MCCI Test in the ACE Program," *Proceedings of Second OECD (NEA) CSNI Specialist Meeting on Molten Core Debris-Concrete Interactions*, Karlsruhe, Germany, April 1-3, 1992 pp. 97-110 (1992).
5. B.R. Spencer et al., "Results of MACE Tests M0 and M1, Second OECD-CSNI Specialist Meeting on Molten Core Debris-Concrete Interactions," *Proceedings of Second OECD (NEA) CSNI Specialist Meeting on Molten Core Debris-Concrete Interactions*, Karlsruhe, Germany, April 1-3 1992 pp. 365-381 (1992).
6. M. T. Farmer, S. Lomperski, D. J. Kilsdonk, and R. W. Aeschlimann, "OECD MCCI Project 2-D Core Concrete Interaction (CCI) Tests: Final Report," OECD/MCCI-2005-TR05 (2006).
7. V. Strizhov, V. Kanukova, T. Vinogradova et al., "An Assessment of the CORCON-MOD3 Code Part I: Thermal-Hydraulic Calculations," NUREG/IA-0129, Office of Nuclear Regulatory Research U.S. Nuclear Regulatory Commission Washington, DC 20555-0001 (1996).
8. J.J. Foit, B. Reimann, G. Adroguer et al., "The WECHSL-Mod3 Code: A Computer Program for the Interaction of a Core Melt with Concrete Including the Long Term Behavior - Model Description and User's Manual", , Forschungszentrum Karlsruhe, Technik und Umwelt, FZKA 5522 (1995).
9. M.T. Farmer, "Modeling of Ex-vessel Corium Coolability with the CORQUENCH Code," *Proceedings of 9th International Conference on Nuclear Energy*, Nice, France, April 8-12, 2001 (2001).
10. M. Nie, M. Fischer and G. Lohnert, "Advanced MCCI Modeling Based on Stringent Coupling of

Thermal Hydraulics and Real Solution Thermochemistry in COSACO,” *Proceedings of 10th International Conference on Nuclear Energy*, Arlington, Virginia, USA, April 11-12, 2002 pp. 229-237 (2002).

11. M. Cranga, C. Mun, B. Michel et al., “Status of the Interpretation of Real Material 2D MCCI Experiments with the ASTEC/MEDICIS Code,” *MCCI-OECD seminar*, Cadarache, St-Paul lez Durance, France, October 10-11, 2007 (2007).
12. B. Spindler, B. Tourniaire, and J. M. Seiler, “Simulation of MCCI with the TOLBIAC-ICB Code Based on the Phase Segregation Model,” *Nucl. Eng. Des.* **236**(19-21), pp. 2264–2270 (2006).
13. M. Cranga, L. Ferry, J.F. Haquet et al., “MCCI in An Oxide/Metal Pool: Lessons Learnt from VULCANO, Greene, ABI and BALISE Experiments and Remaining Uncertainties,” *4th European Review Meeting on Severe Accident Research (ERMSAR-2010)*, Bologna, Italy, May 11-12, 2010 (2010).
14. M. Cranga, B. Spindler, E. Dufour et al., “Simulation of Corium Concrete Interaction in 2D Geometry,” *Prog. in Nucl. Energy* **52**, pp.76-83 (2010).
15. S. Koshizuka and Y. Oka, “Moving-Particle Semi-implicit Method for Fragmentation of Incompressible Fluid,” *Nucl. Sci. Eng.* **123**, pp.421-434 (1996).
16. W.X. Tian, Y. Ishiwatari, S. Ikejiri et al. “Numerical Computation of Thermally Controlled Steam Bubble Condensation Using Moving Particle Semi-implicit (MPS) Method,” *Ann. Nucl. Energy* **37**, pp. 5-15 (2010).
17. R.H. Chen, W.X. Tian, G.H. Su et al., “Numerical Investigation on Bubble Dynamics during Flow Boiling Using Moving Particle Semi-implicit Method,” *Nucl. Sci. Eng.* **240**(11), pp. 3830–3840 (2010).
18. G. Li, Y. Oka, M. Furuya, M. Kondo, “Experiments and MPS Analysis of Stratification Behavior of Two Immiscible Fluids,” *Nucl. Eng. Des.* **265**, pp. 210-221 (2013).
19. R.H. Chen, W.X. Tian, G.H. Su et al., “Numerical Investigation on Bubble Condensation and Coalescence of Bubble Pairs Using Moving Particle Semi-implicit Method,” *Chem. Eng. Sci.* **66**(21), pp. 5055-5063 (2011).
20. K. Shibata S. Koshizuka , M. Sakai, K. Tanizawa, “Lagrangian Simulations of Ship-wave Interactions in Rough Seas,” *Ocean Eng.* **42**(3), pp. 13–25 (2012).
21. T. Matsuura and Y. Oka, “MPS Simulation of Spreading Behavior of Molten Materials,” *Proc. of III International Conference on Particle-based Methods-Fundamentals and Applications Particles* (2013).
22. X. Li, W.X. Tian, R.H. Chen et al., “Numerical Simulation on Single Taylor Bubble Rising in LBE Using Moving Particle Method,” *Nucl. Eng. Des.* **265**, pp.227-234 (2013).
23. R.H. Chen and Y. Oka, “Numerical Analysis of Freezing Controlled Penetration Behavior of the Molten Core Debris in an Instrument Tube with MPS,” *Ann. Nucl. Energy* **71**, pp.322–332 (2014).
24. R.H. Chen and Y. Oka, “Numerical Investigation on Melt Freezing Behavior in a Tube by MPS Method,” *Nucl. Eng. Des.* **273**, pp. 440–448 (2014).
25. X. Li and Y. Oka, “Numerical Simulation of the SURC-2 and SURC-4 MCCI Experiments by MPS Method,” *Ann. Nucl. Energy* **73**, pp. 46–52 (2014).
26. T.N. Dinh, M.J. Konovalikhin, and B.R. Sehgal, “Core Melt Spreading on a Reactor Containment Floor,” *Prog. in Nucl. Energy* **36** (4), pp. 405-468 (2000).
27. M. Epstein, “Thermal Hydraulics of Molten Core Concrete Interactions: a Review and Comparison of Heat Transfer Models with Data, Interpretation of Rheological Data, and a Theory for the Onset of Concrete Spallation,” Palo Alto: Electric Power Research Institute (ACEX-TR-21) (1998).
28. T. Sevón, “Molten Core Concrete Interactions in nuclear accidents - theory and design of an experimental facility,” VTT Tiedotteita. Research Notes 2311 (2005).
29. P. Bamforth, D. Chisholm, J. Gibbs, T. Harrison, “Properties of Concrete for use in Eurocode 2,” http://www.sefindia.org/forum/files/properties_of_concrete_for_use_in_eurocode_2_135.pdf (2008).
30. L. Carenini, J.F. Haquet, C. Journeau, “Crust Formation and Dissolution during Corium Concrete Interaction,” *Proceedings of ICAPP*, Nice, France, May 13-18, 2007 (2007).